IEEE Access
Multidisciplinary ⋮ Rapid Review ⋮ Open Access Journal

Received 12 March 2023, accepted 5 April 2023, date of publication 24 April 2023, date of current version 27 April 2023.

Digital Object Identifier 10.1109/ACCESS.2023.3269561

RESEARCH ARTICLE

Diverse Bursting Oscillations in an Asymmetric Memristive Sallen-Key Filter

KE WANG[1], YIZI CHENG[2], (Student Member, IEEE), ZUNBO ZHANG[1], AND FUHONG MIN[1], (Member, IEEE)

[1]School of Electrical and Automation Engineering, Nanjing Normal University, Nanjing 210023, China
[2]School of Computer and Electronic Information, Nanjing Normal University, Nanjing 210023, China

Corresponding author: Fuhong Min (minfuhong@njnu.edu.cn)

This work was supported in part by the National Natural Science Foundation of China under Grant 61971228.

ABSTRACT The asymmetric memristive diode bridge-based Sallen-Key Filter (AMSKF) achieved by introducing an asymmetry diode bridge connected with a capacitor and an inductor to the Sallen-Key Filter, is studied in this paper. Through the analysis of equilibrium point, the stability of the circuit is discussed. Combined with the bifurcation diagram, it can be seen that the negative feedback gain of the Sallen-Key Filter greatly affects the dynamics of the circuit. Diverse dynamical behaviors are discovered by means of phase portraits and Lyapunov exponents, which include six types of typical oscillating behaviors: Period, Quasi-period, Quasi-periodic bursting, Period-2 bursting, Chaotic bursting and Period-1 bursting. Especially, bifurcation mechanisms of various bursting oscillating behaviors are researched by separating the formal equations into two parts, consisting of the fast spiking subsystem and the slow spiking subsystem, based on the fast-slow analysis method. Finally, Multisim experiments are carried out to validate the results of numerical simulations. Compared with the Sallen-Key Filter cascaded with the symmetric memristive diode bridge, the bursting oscillation with larger amplitude and the wider periodic bursting range by adjusting the negative feedback gain are detected.

INDEX TERMS Sallen-key filter, memristive diode bridge, bursting, Andronov–Hopf bifurcation.

I. INTRODUCTION

Memristor, the concept of which was proposed by Leon Chua in 1971 [1], is regarded as a new-type fundamental circuit element apart from resistor, capacitor, and inductor. As is known to all that the four aforementioned fundamental elements can be employed to expressed the relationships among circuit variables, as shown in Fig.1. Memristor whose resistance would vary with respect to the amount of charge flowing through the device fills a gap between the charge and magnetic flux by demonstrating their relationships directly. Particularly, memristors are widely used in nonlinear circuit design [2] and neural network circuit [3], [4].

Working as the most fundamental feature of the circuit components, memristor should appear universally in more objects. In order to implement the function of memristor on account of oscillating circuits based on memristors, equivalent implementation schemes on the basis of mathematical models have been extensively studied. Recently, The memristive diode bridge introduced by Bao and colleagues [5] is one of the most widely used models due to its simple structure and no grounded limitation. Symmetrical

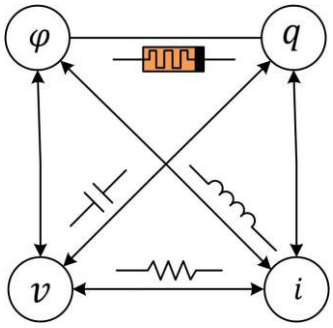

FIGURE 1. The relationships among the four fundamental variables.

The associate editor coordinating the review of this manuscript and approving it for publication was Ludovico Minati.

structure the same as Wheatstone bridge with four diode bridge arms [6], [7], [8], [9] can be observed in the diode bridge-based generic memristive circuit. By selecting different structures, such as the diode bridge cascaded with parallel resistor and capacitor (RC) filter [5], [10], parallel inductor and capacitor (LC) oscillator [11], or hybrid resistor, inductor, and capacitor (RLC) filter [7], [8], [12], [13], several memristive diode bridge emulators with different circuit schematics and dynamical behaviors were proposed. However, symmetry is a special case, while asymmetry is a universal phenomenon. In fact, among items with memristive properties, the pinched hysteresis loops are asymmetric about the origin [14], [15]. Meanwhile, the wave of researches on the phenomenon of symmetric circuit topology in dynamical systems has been stirred [16], [17], [18], [19], [20]. Symmetric memristive diode bridge emulator has been widely employed in nonlinear circuit design.

Bursting oscillations were originally used to describe an important class of electrical dynamical phenomena in biological neurons for information transmission and exchange. Also, bursting oscillations have been discovered in some chaotic circuits based on memristors [21], [22]. A large number of literatures indicate that bursting oscillations are widely found in dynamical systems such as physics, mathematics, and circuits. For example, the pulse sequence bursting oscillation of the fixed-off-time controlled buck converter [23], the coexistence of memristor synaptic coupled adjacent neurons [24], and the periodic and chaotic bursting oscillation of the memristor-based Wien-bridge oscillator and low-pass filter [22], [25]. Bifurcation of nonlinear systems induces it to alternate between quiescent state and spiking state, resulting in multiple modes of bursting oscillations. In [11], the mechanism of various bursting oscillations of the same system is deeply analyzed combined with equilibrium points and Hopf bifurcation. Therefore, studying the mechanism of this specific phenomenon has very important theoretical and physical significance for in-depth understanding of the intrinsic characteristics of the system.

The Sallen-key Filter (SKF) is a topology for designing active filters, a variant of voltage-controlled voltage-source (VCVS) filters, proposed by P. Sallen and E. L. Key at R. Lincoln Laboratory of MIT in 1955. By introducing memristors into classical oscillation circuits or filter circuits, it is easy to realize various nonlinear oscillations and obtain different dynamic behaviors. Memristive circuits have rich dynamic behavior, including chaotic and hyper-chaotic oscillations, symmetric quasi-periodic and chaotic bursting oscillations, symmetric period and chaotic bursting oscillations [22], and coexistence in multi-stable patterns [26]. The structure of the asymmetric diode bridge can bring change to the dynamical behaviors, whereas there are no relevant studies on Sallen-Key circuit currently.

According to the analysis above, the introduction of an asymmetric bridge memristor into the SKF circuit is worth studying. As a result, this paper will focus on the number of diodes on the asymmetric memristive diode bridge, and

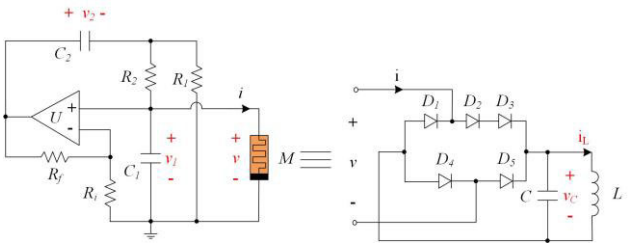

FIGURE 2. Circuit schematic of an asymmetric memristive diode bridge-based sallen-key filter.

one of these situations will be selected to do some researches. The framework of the article will be constructed as follows. In Section II, AMSKF will be built and its mathematical model will be established. In Section III, diverse dynamical behaviors will be discovered by way of phase portraits and Lyapunov exponents, which include several types of typical oscillations. Especially, bifurcation mechanisms of various oscillations will be researched with the increase of the control system parameter. Then, circuit simulations by Multisim will be carried out to confirm numerical simulations in Section IV. Ultimately, the conclusion in line with previous studies will be summarized in Section V.

II. AN ASYMMETRIC MEMRISTIVE DIODE BRIDGE-BASED SALLEN-KEY FILTER

A. MATHEMATICAL MODELING

Different from the Sallen-Key RC filter in the literature [11] and the Wien-bridge bandpass RC filter in literature [22], an improved low-pass filter memristive oscillator circuit is presented based on an asymmetry diode bridge cascaded with a capacitor and a resistor, as depicted in Fig.2. The modified memristive circuit contains dynamic elements of an inverting amplifier, two capacitors, and a voltage-controlled generic memristor, which has a bit of complex circuit topology.

The active voltage-controlled generic memristor is made up of an inductor L, a capacitor C and an asymmetry diode bridge. The terminal topology of circuit is plotted in Fig. 2. The current i flowing through the memristor M, the voltage v of which is numerically equal to the voltage across the capacitor C_1. The current i_L serves as the current flowing along the inductor L. Finally, the mathematical model of M is expressed as

$$\begin{cases} i = I_s e^{\frac{2\rho}{k}(v-v_C)} - I_s e^{-\rho(v+v_C)} \\ C\dfrac{dv_C}{dt} = I_s e^{\frac{2\rho}{k}(v-v_C)} + I_s e^{-\rho(v+v_C)} - 2I_s - i_L \\ L\dfrac{di_L}{dt} = v_c \end{cases} \tag{1}$$

where k is the number of diodes on the asymmetrical bridge arm which contains D_2, D_3 and D_4 in Fig. 2.

In (1), the values of all the elements are listed in Table.1. For the circuit schematic depicted in Fig.1, v_1, v_2 and v_C are the state variables representing the terminal voltages of three

TABLE 1. Circuit parameters of the electronic elements.

Parameters	Definition	Values
C	The capacitor	$470nF$
C_1 C_2	The capacitors	$47nF$
L	The inductor	$20mH$
R_i	The resistor	$3k\Omega$
R_1 R_2	The resistors	200Ω
I_s	The reverse current	$5.84\ nA$
n	The emission coefficient	1.94
V_T	The thermal voltage	$25mV$

capacitors C_1, C_2 and C. In conformity with the Kirchhoff laws, the equations of the AMSKF are given in (2).

$$\begin{cases} C_1\dfrac{dv_1}{dt} = \dfrac{k_1v_1 - v_2}{R_2} - I_s[e^{\frac{2\rho}{k}(v-v_C)} + e^{-\rho(v+v_C)}] \\ C_2\dfrac{dv_2}{dt} = \dfrac{k_1v_1 - v_2}{R_2} + \dfrac{(k_1+1)\,v_1 - v_2}{R_1} \\ C\dfrac{dv_C}{dt} = I_se^{\frac{2\rho}{k}(v-v_C)} + I_se^{-\rho(v+v_C)} - 2I_s - i_L \\ L\dfrac{di_L}{dt} = v_c \end{cases} \tag{2}$$

where $v = v_1$ and $k_1 = R_f/R_i$.

Since two adjustable resistors R_f and R_i affect the negative feedback gain k_1 of SKF, this article focuses on diverse oscillation behaviors with the growth of the individual parameter k_1. For the purpose of enabling the circuit to generate oscillations, the negative feedback gain k_1 of the AMSKF should be greater than 2. As a result of this, the value range of k_1 is determined as (2, 2.6], in the purpose of achieving good results. Other related parameters are listed in Table 1, among which $R_i = 3k\Omega$, $R = R_1 = R_2 = 200\Omega$, $C_1 = C_2 = 47nF$, $C = 470nF$, $L = 20mH$, the parameters of five diodes are chosen as $\rho = 1/2nV_T = 10.3093V^{-1}$ and $I_s = 5.84nA$ by referring to [13].

In order to obtain the dimensionless equations of the circuit equations (2) and decline the number of system parameters, define

$$\begin{aligned} &x = \rho v_1, y = \rho v_2, z = \rho v_c, \tau = t/RC \\ &a = \frac{C}{C_1}, b = \rho RI_s, r = R^2C/L \end{aligned} \tag{3}$$

After dimensionless processing, AMSKF can be expressed by substituting (3) into (2) as

$$\begin{cases} \dot{x} = a\,(k_1x - y) - ab\left[e^{\frac{2}{k}(x-z)} - e^{-(x+z)}\right] \\ \dot{y} = a\,(2k_1+1)\,x - 2ay \\ \dot{z} = b\left[e^{\frac{2}{k}(x-z)} + e^{-(x+z)}\right] - 2b - w \\ \dot{w} = rz \end{cases} \tag{4}$$

where the normalized system parameters in (4) can be obtained from (3) as

$$a = 10, b = 1.0241 \times 10^{-5}, r = 0.94$$

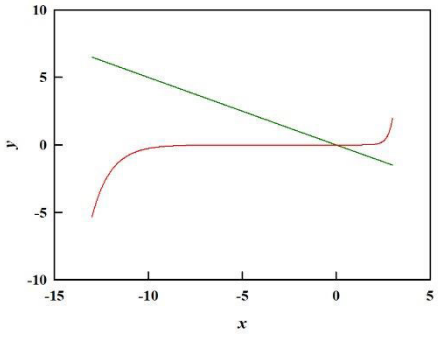

FIGURE 3. The result of graphical analysis on $y_1 = -0.5x$ and $y_2 = b\left(e^{\frac{2}{k}\bar{x}} + e^{-\bar{x}}\right)$.

$$k_1 = (2, 2.6], k = 3 \tag{5}$$

Moreover, as is illustrated in (4), three parameters dominate the system, including a, r, k_1. In this paper, changes of k_1 are the main object of research.

B. EQUILIBRIUM POINT

Let the left side of the dimensionless equation be 0 to obtain the following equations

$$\begin{cases} 0 = a\,(k_1x - y) - ab\left[e^{\frac{2}{k}(x-z)} - e^{-(x+z)}\right] \\ 0 = a\,(2k_1+1)\,x - 2ay \\ 0 = b\left[e^{\frac{2}{k}(x-z)} + e^{-(x+z)}\right] - 2b - w \\ 0 = rz \end{cases} \tag{6}$$

Suppose that the equilibrium point is $P\,(\bar{x}, \bar{y}, \bar{z})$, which is the solution of (6). Thus, we can get the equilibrium point of (4)

$$P = \left[\bar{x},\ (k_1+0.5)\,\bar{x},\ 0,\ b\left(e^{\frac{2}{k}\bar{x}} + e^{-\bar{x}} - 2\right)\right] \tag{7}$$

where $\bar{x}$ is the solution of the following equation

$$0.5\bar{x} + b\left(e^{\frac{2}{k}\bar{x}} + e^{-\bar{x}}\right) = 0 \tag{8}$$

Obviously, by letting $y_1 = -0.5x$, $y_2 = b\left(e^{\frac{2}{k}\bar{x}} + e^{-\bar{x}}\right)$, it can easily be obtained that both are monotonic functions. From Fig.3, it can be inferred that there is only one intersection. Therefore, (8) only has one real root, indicating that the system (4) only has one equilibrium point $P_0 = (0, 0, 0, 0)$.

Correspondingly, the simplified Jacobian matrix at the equilibrium point P_0 can be expressed as

$$J = \begin{bmatrix} ak_1 - ab\left(\frac{2}{k}+1\right) & -a & -ab\left(-\frac{2}{k}+1\right) & 0 \\ a\,(2k_1+1) & -2a & 0 & 0 \\ b\left(\frac{2}{k}-1\right) & 0 & b\left(-\frac{2}{k}-1\right) & -1 \\ 0 & 0 & r & 0 \end{bmatrix} \tag{9}$$

With the chosen parameters, the zero equilibrium point P_0, an unstable saddle-focus, always has two pairs of complex

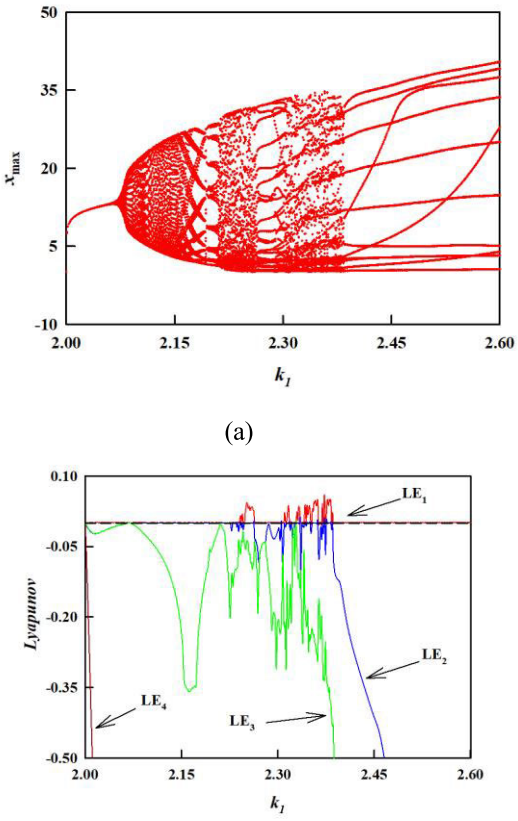

FIGURE 4. Dynamics with varying control parameter k_1 (a) bifurcation diagram of the variable x (b) Lyapunov exponents.

roots with two positive real parts and two negative real parts, respectively.

III. DIVERSE OSCILLATING BEHAVIORS

In this part, Runge-Kutta ODE45 algorithm with the 'AbsTol' and 'RelTol' set to 10^{-10} and 10^{-10} and Wolf's method where the time interval for calculating the finite time Lyapunov exponents is set as 0.0012 s are employed for numerical simulations. The phase portraits, bifurcation diagrams, Lyapunov exponents and Poincare maps are combined together to analyze typical oscillating behaviors and corroborate mutually. With the help of methods aforementioned, various dynamical behaviors of AMSKF are displayed and researched in detail.

A. TYPICAL OSCILLATIONS

First of all, the initial values which is set as $(0, 0.1, 0, 0)$ is chosen as a typical example. The figures evolve with k_1 are shown in Fig.4, Fig.5 and Fig.6.

Deduced from Fig.4, the relevant parameters and the locations of figures about periodic and quasi-periodic oscillations as well as quasi-periodic, periodic or chaotic bursting have been listed in Table 2. Split the interval into seven parts, as shown in Fig.4(a). Compared with symmetrical memristive diode bridges [11], the region of chaotic behavior decreases,

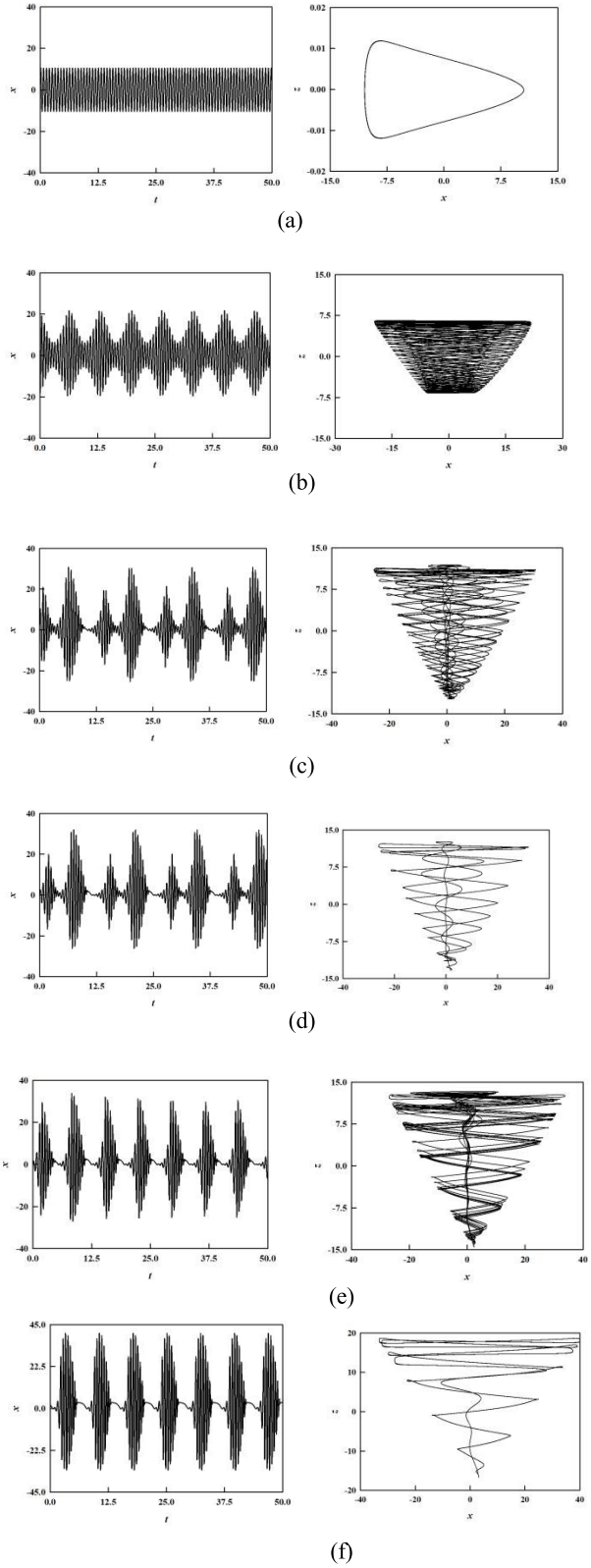

FIGURE 5. Time series and phase trajectories in x-z plane for different k_1:(a) $k_1 = 2.01$ (b) $k_1 = 2.1$ (c) $k_1 = 2.23$ (d) $k_1 = 2.27$ (e) $k_1 = 2.38$ (f) $k_1 = 2.6$.

and by increasing the number of diodes on the asymmetric bridge, an increase in the amplitude of $x_{\max}$ can be observed

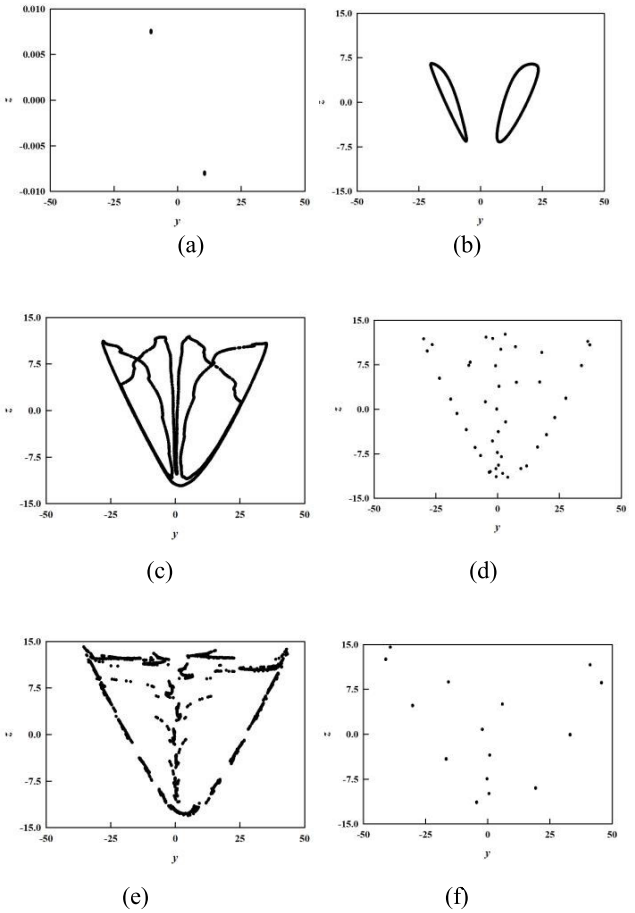

FIGURE 6. Poincare mapping with different k_1:(a) $k_1 = 2.01$ (b) $k_1 = 2.1$ (c) $k_1 = 2.23$ (d) $k_1 = 2.27$ (e) $k_1 = 2.38$ (f) $k_1 = 2.6$.

from the bifurcation plots. Before $k_1 = 2.06$, the system is in a periodic oscillation state at the beginning. Based on the Andronov–Hopf bifurcation route and the Lyapunov exponents, it can be seen that in the range of $2.06 < k_1 < 2.145$, the values of Lyapunov exponents are characterized as $(0, 0, -, -)$, indicating that quasi-periodic oscillation happens. In the region of $2.145 < k_1 < 2.25$, quasi-periodic bursting oscillation occurs with two negative Lyapunov exponents. However, compared with quasi-periodic oscillations, in the range of quasi-periodic bursting oscillations, it is clear that there is silence from the time series. Within the scope of $2.31 < k_1 < 2.38$, system (4) takes on chaotic bursting where Lyapunov exponents are $(+, 0, -, -)$. In addition to the above four cases, periodic bursting also occurs, which includes period-1 bursting and period-2 bursting with a zero maximum Lyapunov exponents and three negative ones. Ultimately, after $k_1 = 2.4$, period-1 bursting can be observed.

Correspondingly, the time sequences of each behavior for various x are plotted in Fig.5, which corresponds to the six typical oscillation behaviors in Table 2. Although the time series when k_1 takes two points 2.23 and 2.27 look like the same, it can be obtained by numerical observation that the peak value is different in different bursting spikes in Fig.5(c) and the peak value is almost the same in different bursting spikes in Fig.5(d). To better distinguish the two phenomena accurately, it is necessary to refer to Lyapunov exponents and Poincare maps. In the range of quasi-periodic bursting, Lyapunov exponents have two zero values and two negative values, while period-2 bursting oscillation only has one zero Lyapunov exponent and three negative Lyapunov exponents. Moreover, the limit cycle in Fig.5(b) seems like a bowl, and in Fig.5(c) the attractor takes on a gyroscopic state. The trajectory lines are dense in quasi-periodic conditions and sparse in periodic conditions.

TABLE 2. Typical dynamical behaviors with different k_1.

k_1	Oscillating behaviors	Finite-time Lyapunov exponents	Figures
2.01	Period	0.0006, −0.0199, −0.0197, −0.4317	Figs. 6(a)7(a)
2.1	Quasi-period	0.0006, 0.0003, −0.0352, −3.9424	Figs. 6(b)7(b)
2.23	Quasi-periodic bursting	0.0005, 0.0002, −0.1412, −5.9228	Figs. 6(c)7(c)
2.27	Period-2 bursting	0.0008, −0.0819, −0.1444, −6.7521	Figs. 6(d)7(d)
2.38	Chaotic bursting	0.0480, 0.0001, −0.3662, −10.3634	Figs. 6(e)7(e)
2.6	Period-1 bursting	0.0007,−1.3097, −5.2992, −33.3526	Figs. 6(f)7(f)

Additionally, the Poincare maps [27] on the $x = 0$ section and reveal approaches are taken for further distinguishing the quasi-period and several bursting behaviors, as shown in Fig.6. Obviously, when the system in Fig.2 is in the status of period, there are two points in the Poincare map, such as Fig.6(a). For chaotic circuits, there will theoretically be an infinite number of points on the maps. However, if the points on the section form a line, this phenomenon is called quasi-period oscillations, such as Fig.6(b). Moreover, if the points on the Poincare map form a two-dimensional figure, or even a fractal structure, it can be judged to be a typical chaotic bursting oscillation, such as Fig.6(e). In Fig.6(f), multi-period bursting oscillation happens, where several scatter points are presented in the image.

It is remarkable that when $k_1 \leq 2$, the AMSKF falls short of the condition of self-excited oscillation, so we start from $k_1 = 2$. In particular, from the time series of state variables x and z, x appears as a fast-scale bursting oscillation change, while z appears as a slow-scale oscillation change, indicating that (4) can be divided into fast and slow subsystems.

B. BIFURCATION MECHANISM OF SLOW CHANNEL EFFECT

In the time series, there is a significant difference between the envelope change of the fast variable x and the change of the

slow variable z, which is caused by the slow passage effect of the memristive filter circuit.

It is easy to see that the parameter b is approximately six times smaller than the parameter a. Based on the fast-slow analysis method, the two parts of the equation divided from the system can be obtained separately. The fast subsystem is

$$\begin{cases} \dot{x} = a\left(k_1 x - y\right) - ab\left[\mathrm{e}^{\frac{2}{k}(x-z)} - \mathrm{e}^{-(x+z)}\right] \\ \dot{y} = a\left(2k_1 + 1\right)x - 2ay \end{cases} \tag{10a}$$

and the other slow subsystem which is described as

$$\begin{cases} \dot{z} = b\left[\mathrm{e}^{\frac{2}{k}(x-z)} + \mathrm{e}^{-(x+z)}\right] - 2b - w \\ \dot{w} = rz \end{cases} \tag{10b}$$

The slow subsystem is coupled to the fast subsystem via the slow variable z between the two 2-dimensional(2-D) subsystems. Therefore, in (10a), the slow variable z can be viewed as a specific parameter. The equilibrium point of (10a) can be derived as

$$E_{FS} = \left[\hat{x},\, (k_1{+}0.5)\,\hat{x}\right] \tag{11}$$

where $\hat{x}$ can be obtained by solving the simultaneous equations (10a) and (11)

$$0.5\hat{x} + b\left(\mathrm{e}^{\frac{2}{k}(\hat{x}-z)} + \mathrm{e}^{-(\hat{x}+z)}\right) = 0 \tag{12}$$

Meanwhile, the characteristic equation at E_{FS} can be depicted as

$$P\left(\lambda\right) = \lambda^2{+}\mathrm{A}\lambda + B \tag{13}$$

where $\mathrm{A} = a\left[2 - k_1 + b\left(\frac{2}{k}\mathrm{e}^{\frac{2}{k}(x-z)} + \mathrm{e}^{-(\mathrm{x}+z)}\right)\right]$, $B = a^2\left[1 + 2b\left(\frac{2}{k}\mathrm{e}^{-\frac{2}{k}z} + \mathrm{e}^{-z}\right)\right]$.

Since $a, b, k > 0$, the following inequality is always satisfied,

$$a^2\left[1 + 2b\left(\frac{2}{k}\mathrm{e}^{-\frac{2}{k}z} + \mathrm{e}^{-z}\right)\right] > 0 \tag{14}$$

indicating that (13) has no zero eigenvalues. Thus, there is no fold bifurcation point in the fast subsystem. When the condition (15) is satisfied, Hopf bifurcation appears with a pair of pure imaginary eigenvalues, which demonstrates that the Hopf bifurcation set is the same as (15).

$$2 - k_1 + b\left(\frac{2}{k}\mathrm{e}^{\frac{2}{k}(x-z)} + \mathrm{e}^{-(\mathrm{x}+z)}\right) = 0 \tag{15}$$

When the control parameter k_1 is determined, the Hopf bifurcation value of the slow variable z can be modalized by solving transcendental equations (12) and (15). In order to clarify the oscillation mechanism in the TABLE 2, special cases where $k_1 = 2.1$ and $k_1 = 2.6$ are taken as examples. Through the simulations in MATLAB, the unique solution is obtained. When $k_1 = 2.1$, it can be calculated that $z = -8.9605$. Likewise, when $k_1 = 2.6$, it can be calculated that $z = -9.7728$.

If the amplitude of the waveform z is higher than the value of the Hopf bifurcation plane, which means that the characteristic equation has a solution of the eigenroot with a real part greater than 0, indicating that the system is unstable and the bursting oscillation state of the fast variable x is caused by the slow variable z. Conversely, if the amplitude of the waveform z is lower than the value of the Hopf bifurcation plane, which denotes that the system is in the quiescent state. Similarly, when the waveform of the variable z crosses the Hopf bifurcation plane, to put it another way, z passes through the Hopf bifurcation point, the real part of the eigenroot changes from positive to negative, indicating that the stability of the equilibrium point E_{FS} evolves from unstable to stable.

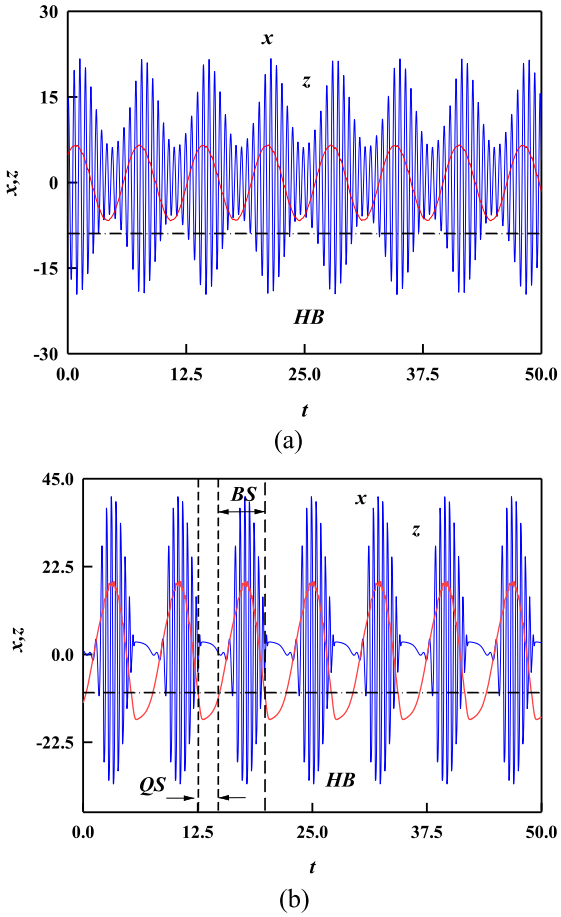

FIGURE 7. Bifurcation analyses (a) $k_1 = 2.1$, quasi-periodic oscillation, $z = -8.9605$, (b) $k_1 = 2.6$, period-1 bursting oscillation, $z = -9.7728$.

TABLE 3. Comparison between the symmetric and asymmetric circuits.

Differences	Symmetrical diode bridge	Asymmetric diode bridge
Model of memristor	Symmetric memristive diode bridge-based Sallen-Key Filter	Asymmetric memristive diode bridge-based Sallen-Key Filter
Phenomena	The bursting oscillation with longer silence and wider chaotic bursting range	The bursting oscillation with larger amplitude and wider periodic bursting range

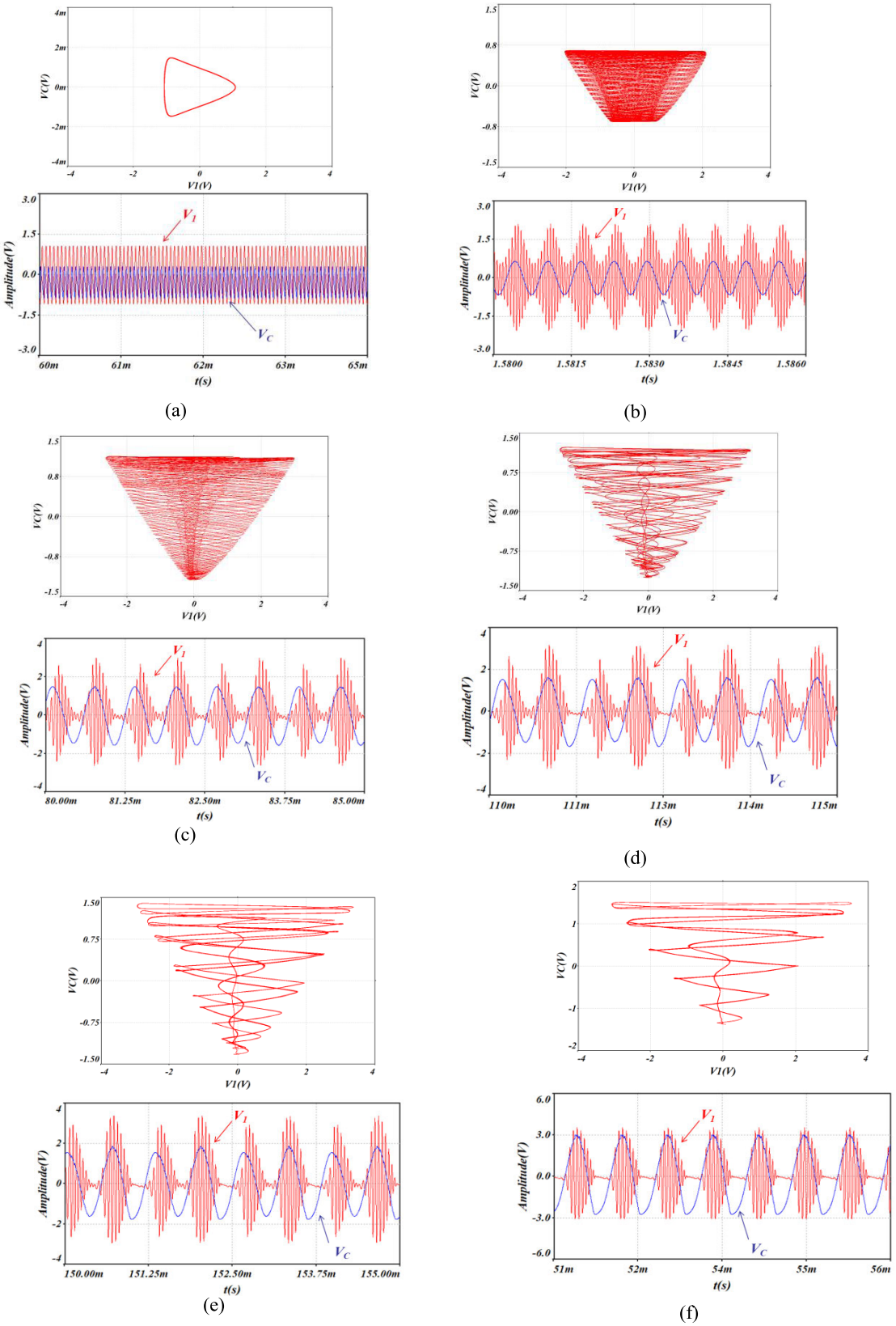

FIGURE 8. Multisim simulations with different R_f (a) period oscillation at $R_f = 6.03k\Omega$ (or $k_1 = 2.01$) (b) quasi-period oscillation at $R_f = 6.3k\Omega$(or $k_1 = 2.1$) (c) quasi-period bursting at $R_f = 6.69k\Omega$ (or $k_1 = 2.23$) (d) period-2 bursting at $R_f = 6.81k\Omega$ (or $k_1 = 2.27$) (e)chaotic bursting at $R_f = 7.14k\Omega$ (or $k_1 = 2.38$) (f) period-1 bursting at $R_f = 7.8k\Omega$(or $k_1 = 2.6$).

As a result, the fast variable transits from a bursting state (BS) to a quiescence state (QS), such as the the intervals of a bursting state (BS) and a quiescence state (QS) shown in Fig.7(b).

At the point of $k_1 = 2.1$, the timing diagram of the quasi-periodic oscillation is drawn in Fig.7(a), under the situation of which, it can be calculated that $z = -8.9605$. As is shown apparently in Fig.7(a), the solid red line represents the timing diagram of the variable z, and the black dotted line represents the Hopf bifurcation plane. Glancing from it, there is no intersection between the solid red line and the black dotted line, and the solid red line is always above the black dotted line, indicating that no Hopf bifurcation occurs and the system is always in a state of bursting oscillation.

According to the analysis above, Table 3 is listed below to compare the differences between the symmetric memristive circuit and the asymmetric memristive circuit.

IV. CIRCUIT VERIFICATION

Following the above theoretical analysis, in order to verify the numerical simulation results of the circuit schematics, digital circuit experiments are carried out. According to the circuit schematics in Fig.2, the terminal circuit parameters in Table 1, the AMSKF is easily established. The circuit is built with AD711KN, an integrated operational amplifier supplied with a symmetric ±15 V DC voltage power. What's more, diodes of the same specification 1N4148 whose parameters are selected as $\rho = 1/2nV_T = 10.3093V^{-1}$ and $I_s = 5.84nA$ are chosen for bridge arms. Other basic electrical components are four resistors, three capacitors, and one inductor whose values are $R_i = 3k\Omega$, $R_1 = R_2 = 200\Omega$, $C_1 = C_2 = 47nF$, $C = 470nF$ and $L = 20mH$, respectively. The experimental results are gotten by adjusting the resistor R_f to increase k_1 in Multisim14.1. The experimental time series as well as phase portraits in plane $x - z$ are captured on the oscilloscope, as shown in Fig.8, which are exactly the same to Fig.5.

V. CONCLUSION

In this article, through adding an asymmetry diode bridge cascaded with a capacitor and a resistor to the Sallen-Key Filter, AMSKF was designed. Circuit schematic and its equilibrium stability analysis were carried out along with dynamics were investigated comprehensively by numerical simulations and experimental measurements. In particular, bifurcation mechanisms with respect to its parameter of various bursting oscillating behaviors in AMSKF were characterized with the method of fast-slow analysis. Compared with the symmetric memristive diode bridge-based Sallen-Key Filter, the bursting oscillation with larger amplitude and the wider periodic bursting range by adjusting the negative feedback gain were detected in AMSKF. In addition, the built model can be further extended by varying the number of diodes on the diode-bridge arm or exploring in high-pass Sallen-Key Filter.

REFERENCES

[1] L. Chua, "Memristor—The missing circuit element," *IEEE Trans. Circuit Theory*, vol. CT-18, no. 5, pp. 507–519, Sep. 1971, doi: 10.1109/TCT.1971.1083337.

[2] F. Min and L. Xue, "Routes toward chaos in a memristor-based Shinriki circuit," *Chaos, Interdiscipl. J. Nonlinear Sci.*, vol. 33, no. 2, Feb. 2023, Art. no. 023122, doi: 10.1063/5.0126900.

[3] J. Sun, G. Han, Z. Zeng, and Y. Wang, "Memristor-based neural network circuit of full-function Pavlov associative memory with time delay and variable learning rate," *IEEE Trans. Cybern.*, vol. 50, no. 7, pp. 2935–2945, Jul. 2020, doi: 10.1109/TCYB.2019.2951520.

[4] J. Sun, Y. Wang, P. Liu, S. Wen, and Y. Wang, "Memristor-based neural network circuit with multimode generalization and differentiation on Pavlov associative memory," *IEEE Trans. Cybern.*, early access, Sep. 21, 2022, doi: 10.1109/TCYB.2022.3200751.

[5] B. Bao, J. Yu, F. Hu, and Z. Liu, "Generalized memristor consisting of diode bridge with first order parallel RC filter," *Int. J. Bifurcation Chaos*, vol. 24, no. 11, Nov. 2014, Art. no. 1450143, doi: 10.1142/S0218127414501430.

[6] Q. Xu, Q. L. Zhang, B. C. Bao, and Y. H. Hu, "Non-autonomous second-order memristive chaotic circuit," *IEEE Access*, vol. 5, pp. 21039–21045, 2017, doi: 10.1109/ACCESS.2017.2727522.

[7] B. Bao, L. Xu, N. Wang, H. Bao, Q. Xu, and M. Chen, "Third-order RLCM-four-elements-based chaotic circuit and its coexisting bubbles," *AEU-Int. J. Electron. Commun.*, vol. 94, pp. 26–35, Sep. 2018, doi: 10.1016/j.aeue.2018.06.042.

[8] Q. Xu, Q. L. Zhang, H. Qian, H. G. Wu, and B. C. Bao, "Crisis-induced coexisting multiple attractors in a second-order nonautonomous memristive diode bridge-based circuit," *Int. J. Circuit Theory Appl.*, vol. 46, no. 10, pp. 1917–1927, Oct. 2018, doi: 10.1002/cta.2492.

[9] S. K. Tchiedjo, L. K. Kengne, J. Kengne, and G. D. Kenmoe, "Dynamical behaviors of a chaotic jerk circuit based on a novel memristive diode emulator with a smooth symmetry control," *Eur. Phys. J. Plus*, vol. 137, no. 8, p. 940, Aug. 2022, doi: 10.1140/epjp/s13360-022-03165-w.

[10] J. Kengne, Z. N. Tabekoueng, V. K. Tamba, and A. N. Negou, "Periodicity, chaos, and multiple attractors in a memristor-based Shinriki's circuit," *Chaos, Interdiscipl. J. Nonlinear Sci.*, vol. 25, no. 10, Oct. 2015, Art. no. 103126, doi: 10.1063/1.4934653.

[11] H. Wu, Y. Ye, M. Chen, Q. Xu, and B. Bao, "Extremely slow passages in low-pass filter-based memristive oscillator," *Nonlinear Dyn.*, vol. 97, no. 4, pp. 2339–2353, Sep. 2019, doi: 10.1007/s11071-019-05131-1.

[12] F. Corinto and A. Ascoli, "Memristive diode bridge with LCR filter," *Electron. Lett.*, vol. 48, no. 14, p. 824, 2012, doi: 10.1049/el.2012.1480.

[13] B.-C. Bao, P. Wu, H. Bao, M. Chen, and Q. Xu, "Chaotic bursting in memristive diode bridge-coupled Sallen-Key lowpass filter," *Electron. Lett.*, vol. 53, no. 16, pp. 1104–1105, Aug. 2017, doi: 10.1049/el.2017.1647.

[14] W. Xue, W. Ci, X.-H. Xu, and G. Liu, "Optoelectronic memristor for neuromorphic computing," *Chin. Phys. B*, vol. 29, no. 4, Apr. 2020, Art. no. 048401, doi: 10.1088/1674-1056/ab75da.

[15] H. Wu, J. Zhou, M. Chen, Q. Xu, and B. Bao, "DC-offset induced asymmetry in memristive diode-bridge-based Shinriki oscillator," *Chaos, Solitons Fractals*, vol. 154, Jan. 2022, Art. no. 111624, doi: 10.1016/j.chaos.2021.111624.

[16] J. Gu, C. Li, Y. Chen, H. H. C. Iu, and T. Lei, "A conditional symmetric memristive system with infinitely many chaotic attractors," *IEEE Access*, vol. 8, pp. 12394–12401, 2020, doi: 10.1109/ACCESS.2020.2966085.

[17] J. Ramadoss, J. Kengne, A. N. K. Telem, and K. Rajagopal, "Broken symmetry and dynamics of a memristive diodes bridge-based Shinriki oscillator," *Phys. A, Stat. Mech. Appl.*, vol. 588, Feb. 2022, Art. no. 126562, doi: 10.1016/j.physa.2021.126562.

[18] M. Hua, H. Wu, Q. Xu, M. Chen, and B. Bao, "Asymmetric memristive Chua's chaotic circuits," *Int. J. Electron.*, vol. 108, no. 7, pp. 1106–1123, Jul. 2021, doi: 10.1080/00207217.2020.1819440.

[19] Y. Ye, J. Zhou, Q. Xu, M. Chen, and H. Wu, "Parallel-type asymmetric memristive diode-bridge emulator and its induced asymmetric attractor," *IEEE Access*, vol. 8, pp. 156299–156307, 2020, doi: 10.1109/ACCESS.2020.3018728.

[20] F. Li, T. Wang, M. Chen, and H. Wu, "A unified asymmetric memristive diode-bridge emulator and hardware confirmation," *Eur. Phys. J. Special Topics*, vol. 230, nos. 7–8, pp. 1805–1811, Aug. 2021, doi: 10.1140/epjs/s11734-021-00180-3.

[21] B. C. Bao, P. Jiang, H. Wu, and F. Hu, "Complex transient dynamics in periodically forced memristive Chua's circuit," *Nonlinear Dyn.*, vol. 79, no. 4, pp. 2333–2343, Mar. 2015, doi: 10.1007/s11071-014-1815-1.
[22] H. Wu, B. Bao, Z. Liu, Q. Xu, and P. Jiang, "Chaotic and periodic bursting phenomena in a memristive Wien-bridge oscillator," *Nonlinear Dyn.*, vol. 83, nos. 1–2, pp. 893–903, Jan. 2016, doi: 10.1007/s11071-015-2375-8.
[23] X. Zhang, J. Xu, B. Bao, and G. Zhou, "Asynchronous-switching map-based stability effects of circuit parameters in fixed off-time controlled buck converter," *IEEE Trans. Power Electron.*, vol. 31, no. 9, pp. 6686–6697, Sep. 2016, doi: 10.1109/TPEL.2015.2501367.
[24] H. Bao, W. B. Liu, and A. H. Hu, "Coexisting multiple firing patterns in two adjacent neurons coupled by memristive electromagnetic induction," *Nonlinear Dyn.*, vol. 95, no. 1, pp. 43–56, Jan. 2019, doi: 10.1007/s11071-018-4549-7.
[25] B. C. Bao, P. Y. Wu, H. Bao, Q. Xu, and M. Chen, "Numerical and experimental confirmations of quasi-periodic behavior and chaotic bursting in third-order autonomous memristive oscillator," *Chaos, Solitons Fractals*, vol. 106, pp. 161–170, Jan. 2018, doi: 10.1016/j.chaos.2017.11.025.
[26] C. J. Chen, J. Q. Chen, H. Bao, M. Chen, and B. C. Bao, "Coexisting multistable patterns in memristor synapse-coupled Hopfield neural network with two neurons," *Nonlinear Dyn.*, vol. 95, no. 4, pp. 3385–3399, Mar. 2019, doi: 10.1007/s11071-019-04762-8.
[27] Z. Galias, "Simulations of memristors using the Poincaré map approach," *IEEE Trans. Circuits Syst. I, Reg. Papers*, vol. 67, no. 3, pp. 963–971, Mar. 2020, doi: 10.1109/TCSI.2019.2949736.

KE WANG is currently pursuing the bachelor's degree with the School of Electrical and Automation Engineering, Nanjing Normal University, China. His current research interests include chaotic systems and memristive circuits.

YIZI CHENG (Student Member, IEEE) received the M.E. degree in electrical engineering from Nanjing Normal University, Nanjing, China, in 2022, where he is currently pursuing the Ph.D. degree in physical electronics. His research interests include chaotic systems and memristive circuits.

ZUNBO ZHANG is currently pursuing the bachelor's degree with the School of Electrical and Automation Engineering, Nanjing Normal University, China. His current research interests include chaotic systems and memristive circuits.

FUHONG MIN (Member, IEEE) received the master's degree from the School of Communication and Control Engineering, Jiangnan University, in 2003, and the Ph.D. degree from the School of Automation, Nanjing University of Science and Technology, in 2007. From 2009 to 2010, she was a Postdoctoral Fellow with the School of Mechanical Engineering, University of Southern Illinois. She is currently a Professor with the School of Electrical and Automation Engineering, Nanjing Normal University. Her research interests include memristive circuits, control and synchronization of chaotic circuits, and complex behavior of nonlinear power electronic circuits.